Solid State Communications 405 (2025) 116135

Contents lists available at ScienceDirect

Solid State Communications

journal homepage: www.elsevier.com/locate/ssc

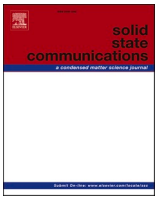

Experimental and simulation study of Cu_2O-based heterojunction solar cells: Effects of bath temperature, layer thickness and defect density

Abdelghani Rahal [a,b], Idris Bouchama [a,b], M.A. Ghebouli [a,c], B. Ghebouli [d], M. Fatmi [a,*], Talal M. Althagafi [e,**], S. Boudour [f]

[a] Research Unit on Emerging Materials (RUEM), University Ferhat Abbas, Setif1, Algeria
[b] Department of electronics, Faculty of Technology, University of M'sila, 28000, M'sila, Algeria
[c] Department of Chemistry, Faculty of Sciences, University of M'sila, University Pole, Road Bourdj Bou Arreiridj, 28000, M'sila, Algeria
[d] Laboratory for the Study of Surfaces and Interfaces of Solid Materials (LESIMS), University Ferhat Abbas of Setif 1, Setif, 19000, Algeria
[e] Department of Physics, College of Science, Taif University, Taif, 21944, Saudi Arabia
[f] Research Center in Industrial Technologies CRTI, P.O. Box 64, Cheraga, Algiers, 16014, Algeria

ARTICLE INFO

Communicated by: Saha Bivas

Keywords:
Cu_2O thin films
Electrochemical deposition
Bath temperature
SCAPS simulation
Photovoltaic performance

ABSTRACT

This research paper presents a comprehensive study of Cu_2O-based heterojunction solar cells, focusing on the effects of bath temperature, absorber layer thickness, and defect density on cell efficiency. Cu_2O thin films were electrochemically deposited at various bath temperatures (40–80 °C), and their structural and optical properties were investigated. Performance simulations using SCAPS software revealed that the optimal Cu_2O layer thickness is 4 μm, yielding a conversion efficiency of 12.1 %. Under optimal conditions (bath temperature 60 °C and absorber thickness 4 μm), the device achieved a simulated efficiency of 12.6 %. Results demonstrated that moderate acceptor density (10^{17} cm^{-3}) and low defect density (10^{14} cm^{-3}) lead to significant improvements in cell efficiency. This study provides valuable insights for developing high-efficiency Cu_2O/CdS/ZnO solar cells, emphasizing the importance of controlling deposition parameters and layer design for enhanced performance of copper oxide-based photovoltaics.

1. Introduction

Humanity faces increasing challenges in the energy sector, driving researchers toward developing sustainable and environmentally friendly alternative energy sources. Solar cells are among the most promising renewable energy technologies, offering the possibility of directly converting sunlight into electrical energy [1]. In recent decades, silicon cells have dominated the solar cell market, but high production costs and complex manufacturing processes have encouraged researchers to explore alternative materials [2].Cuprous oxide (Cu_2O) is considered a promising material for solar cell applications due to its ideal physical and electrical properties [3]. Cu_2O features a direct bandgap ranging from 1.9 to 2.2 eV, a high optical absorption coefficient, along with the abundance of copper in the Earth's crust and its low toxicity [4]. Theoretically, Cu_2O solar cells can achieve conversion efficiencies of up to 20 % according to the Shockley-Queisser limit, making them strong competitors to conventional solar cell technologies [5]. In recent years, various Cu_2O deposition methods have been developed, including thermal spray, chemical vapor deposition, metallic copper oxidation, and electrochemical deposition [6]. Among these methods, electrochemical deposition offers several advantages, including low required temperature, easy control of the deposited layer thickness, low cost, and the ability to deposit on large areas [7]. Recent studies have shown that the properties of electrochemically deposited Cu_2O layers are significantly affected by several factors, including bath temperature, current density, and solution pH [8]. To improve the performance of Cu_2O solar cells, various heterojunction structures such as Cu_2O/ZnO and Cu_2O/CdS have been developed [9]. The window layer and buffer layer play critical roles in cell efficiency by reducing carrier recombination at the interface [10]. Studies have shown that the Cu_2O/CdS/ZnO structure can achieve higher conversion efficiency due to the good match in energy levels between the different materials [11]. Despite significant progress in developing Cu_2O solar cells, the conversion efficiency recorded in laboratories (around 8 %) remains much

* Corresponding author.
** Corresponding author.
E-mail addresses: fatmimessaoud@yahoo.fr (M. Fatmi), t.althagafi@tu.edu.sa (T.M. Althagafi).

https://doi.org/10.1016/j.ssc.2025.116135
Received 17 July 2025; Received in revised form 17 August 2025; Accepted 2 September 2025
Available online 3 September 2025

lower than the theoretical limit [12]. This is due to several challenges, including the instability of Cu_2O under different deposition conditions, the presence of crystalline defects, and non-optimal charge carrier concentration [13]. These limitations highlight the main challenges of Cu_2O solar cells: high defect densities that act as recombination centers, instability under varying growth conditions, and difficulties in precisely controlling acceptor density during electrodeposition. In this study, we address these issues by integrating experimental electrochemical deposition with SCAPS-1D simulations, thereby establishing direct links between deposition parameters and both material properties and device performance. This dual approach provides new insights compared to previous works. Therefore, it is essential to understand the effect of different deposition parameters on the structural, electrical, and optical properties of Cu_2O layers and consequently on the performance of the solar cell.Recent studies have shown that the bath temperature significantly affects the structure, crystal orientation, and grain size in Cu_2O layers [14]. Han et al. (2023) found that increasing the bath temperature from 30 to 60 °C leads to a significant improvement in the electrical conductivity of Cu_2O layers [15]. Additionally, Wang et al. (2022) confirmed that the thickness of the Cu_2O absorber layer has a significant effect on light absorption efficiency and charge carrier collection [16]. Alongside experimental studies, simulation models play an important role in understanding and improving solar cell performance. The SCAPS (Solar Cell Capacitance Simulator) program is an effective tool for modeling and simulating the performance of heterojunction solar cells [17]. Through SCAPS simulation, Ibrahim et al. (2023) identified critical factors affecting the performance of Cu_2O/CdS/ZnO cells, including absorber layer thickness, acceptor concentration, and crystalline defect density [18]. Various techniques have been employed to deposit Cu_2O thin films—including thermal oxidation, magnetron sputtering, pulsed-laser deposition, chemical vapor deposition, and electrochemical deposition each with distinct trade-offs in temperature, vacuum requirements, equipment cost, and throughput [19]. In contrast, **electrodeposition** offers a simple, low-temperature, and scalable route with precise control over film thickness, morphology, texture, and doping via bath chemistry and potential programs [20,21]. Moreover, electrodeposition has been demonstrated on large-area substrates and integrated into low-cost multi-step process flows, underscoring its suitability for manufacturing Cu_2O-based devices [22]. These considerations motivate our choice of electrochemical deposition in this work. This study provides a comprehensive analysis of the effect of electrochemical deposition bath temperature on the structural and optical properties of thin Cu_2O films. Additionally, the SCAPS program was used to simulate the performance of Cu_2O/CdS/ZnO solar cells with a focus on the effect of Cu_2O absorber layer thickness, acceptor density, and defect density on key cell parameters such as open-circuit voltage (Voc), short-circuit current density (Jsc), fill factor (FF), and conversion efficiency (η). This study aims to provide deep insights for improving the design and manufacture of high-efficiency Cu_2O solar cells.

2. Experimental methods

Cu_2O thin films were deposited on conductive substrates using the electrochemical deposition method. Prior to deposition, the substrates were thoroughly cleaned in an ultrasonic bath using acetone, ethanol, and distilled water sequentially. During electrodeposition, a constant potential of −0.4 V **vs.** Ag/AgCl (saturated KCl) was applied using a three-electrode configuration, with a platinum wire as the counter electrode and a saturated Ag/AgCl electrode as the reference. The deposition process was carried out for 30 min to ensure uniform film growth. Fluorine-doped tin oxide (FTO) coated glass substrates with a sheet resistance of ~15 Ω/sq were employed, providing both electrical conductivity during electrodeposition and optical transparency for subsequent characterization. The applied potential was carefully controlled to ensure reproducibility of the Cu_2O film growth. The deposition bath consisted of a 0.4 M copper sulfate ($CuSO_4$) solution and 3 M lactic acid, with the pH adjusted to 12.5 using sodium hydroxide solution. The deposition process was performed at different temperatures 40, 60, and 80 °C under a constant applied electrical potential. After deposition, the structural properties of the films were investigated through X-ray diffraction (XRD) analysis. XRD and UV–Visible measurements were performed on films deposited on FTO-coated glass substrates, which provided both conductivity for electrodeposition and transparency for optical characterization. Optical properties were evaluated using a UV–Visible spectrophotometer to determine the optical bandgap. In addition, cyclic voltammetry and chronoamperometry were employed to analyze the deposition mechanism and assess the influence of bath temperature. Cyclic voltammetry (CV) measurements were carried out in the same three-electrode configuration, using a platinum wire as the counter electrode and a saturated Ag/AgCl electrode as the reference. The scan rate was fixed at 50 mV/**s**, which ensured a stable current response and reproducible electrochemical behavior. To evaluate the potential of these films in photovoltaic applications, solar cell performance was simulated using the SCAPS-1D software. The model focused on Cu_2O/CdS/ZnO solar cells, and the simulations examined the impact of varying the Cu_2O absorber layer thickness (1–7 μm), acceptor density (10^{16}–10^{19} cm^{-3}), and defect density (10^{13}–10^{16} cm^{-3}). The physical parameters used in the simulation are presented in Table 1.

3. Results and discussion

3.1. Cyclic voltammetry analysis

Fig. 1 shows the cyclic voltammetry curves of the substrates, which reveal the reduction and oxidation behavior on the substrate surface. The curve shows a clear reduction peak at about −0.4 V, which represents the reduction of divalent copper ions (Cu^{2+}) to cuprous oxide (Cu_2O). These results are consistent with the study by Zhang et al. (2022), which showed that the Cu_2O deposition process occurs through the reduction of Cu^{2+} and its reaction with hydroxyl ions [23]. The electrochemical growth of Cu_2O thin films proceeds via a two-step reduction process of Cu^{2+} ions in the electrolyte. Initially, Cu^{2+} ions are reduced to Cu^{+} species, which subsequently combine with oxygen ions to form Cu_2O nuclei on the cathode surface. As the deposition continues, these nuclei coalesce and grow into larger crystallites. The bath temperature plays a critical role in this process: at lower temperatures, the nucleation rate is higher, resulting in smaller grains and less preferred orientation, whereas at higher temperatures, enhanced ion mobility promotes improved crystallinity, larger grain size, and a stronger (111) preferential orientation. Such temperature-dependent kinetics explain the observed structural and optical trends in our experimental results.

Table 1
Physical parameters used in the simulation [23–26].

Material properties	Cu_2O	CdS	ZnO
Thickness (μm)	Varied	0.1	0.08
Band gap (eV)	2.17	2.4	3.3
Electron affinity (eV)	3.20	4.2	4.6
Dielectric permittivity (relative)	7.11	10	9
CB (conduction band) effective density of states (cm^{-3})	2.0×10^{17}	2.0×10^{18}	2.2×10^{18}
VB (valence band) effective density of states (cm^{-3})	1.1×10^{19}	1.5×10^{19}	1.8×10^{19}
Electron mobility μ_n (cm^2/V·s)	80	80	80
Hole mobility μ_p (cm^2/V·s)	25	25	25
Shallow uniform donor density N_D (cm^{-3})	0	1.0×10^{17}	1×10^{19}
Shallow uniform acceptor density N_A (cm^{-3})	$1. \times 10^{18}$	1×10^{18}	1×10^{16}

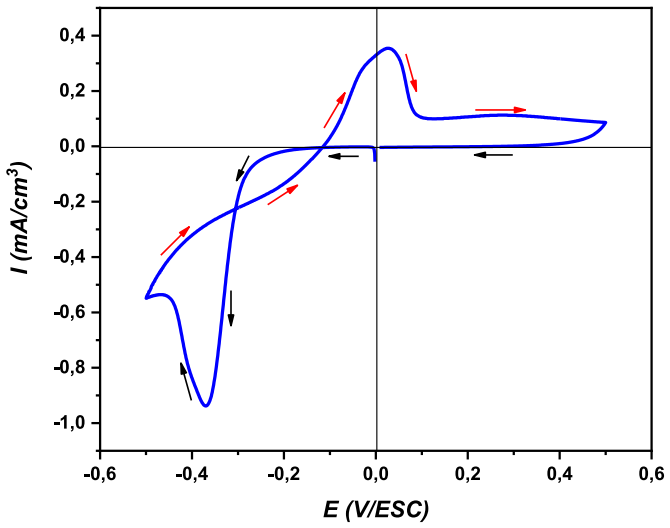

Fig. 1. Substrate cyclic voltammograms.

3.2. Effect of bath temperature on the deposition process

Fig. 2 shows the chronoamperometric curves recorded during the deposition of Cu_2O layers at different temperatures. It is observed that the current density increases significantly with increasing bath temperature, indicating an increased deposition rate. At 60 °C, the highest current density was recorded, which is consistent with the study by Liu et al. (2023), which showed that increasing temperature enhances the kinetics of electrochemical reactions and increases the rate of ion diffusion in the solution [24]. In the chronoamperometric inset of Fig. 2, regions I, II, and III correspond to distinct stages of the electrodeposition process. Region I is associated with the rapid charging of the electrical double layer at the electrode/electrolyte interface. Region II reflects the nucleation of Cu_2O crystallites on the substrate surface. Region III represents the subsequent three-dimensional growth of these nuclei into continuous Cu_2O films. This interpretation is consistent with typical chronoamperometric behavior observed in electrochemical deposition of metal oxides.

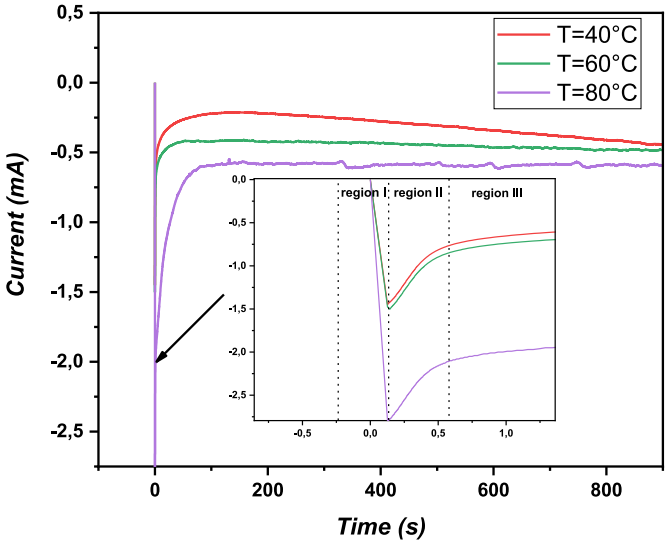

Fig. 2. Typical chronoamperometric curves obtained during Cu_2O thin films electrodeposition at different bath temperatures.

3.3. Structural properties of Cu_2O layers

The X-ray diffraction patterns of Cu_2O layers deposited at different temperatures. All samples show diffraction peaks at 2θ angles of 29.6°, 36.4°, 42.3°, and 61.5°, which correspond to the crystal planes (110), (111), (200), and (220) of the cubic Cu_2O structure. It is observed that the intensity of the (111) peak increases significantly with increasing bath temperature, indicating improved crystallization and increased crystal size (Fig. 3). These results are consistent with Chen et al. (2024), who found that higher bath temperatures lead to improved preferential crystal orientation toward the (111) plane [25]. Quantitative XRD analysis was conducted to strengthen the structure–performance correlation. The average crystallite size (D) was estimated from the (111) peak broadening using the Scherrer equation (K = 0.9, λ = 1.5406 Å), yielding values in the range of 25–65 nm as the bath temperature increased from 40 to 80 °C. The corresponding dislocation density ($\delta = 1/D^2$) decreased from ~1.6×10^{15} cm^{-2} at 40 °C to ~2.4×10^{14} cm^{-2} at 80 °C, indicating improved crystallinity and reduced defect density. These trends are consistent with the enhanced carrier transport inferred from device simulations. To further interpret these results, the physicochemical growth mechanism of Cu_2O films must be considered. At lower deposition temperatures, the nucleation rate is dominant, leading to the formation of smaller crystallites and broader diffraction peaks, which are signatures of high lattice strain and defect density. In contrast, higher bath temperatures enhance ionic mobility and diffusion, promoting coalescence of nuclei into larger grains with sharper and more intense peaks that reflect improved crystallinity and a preferential (111) orientation. From a chemical standpoint, Cu_2O formation proceeds through the reduction of Cu^{2+} to Cu^{+} ions, which subsequently react with oxygen species to generate Cu_2O nuclei that aggregate into crystalline grains. This combined physical and chemical mechanism explains the observed correlation between deposition temperature, crystallinity, and the reduction of structural defects, thereby linking growth conditions to device performance.

3.4. Optical properties of Cu_2O layers

Fig. 4 shows the Tauc plots for Cu_2O layers deposited at different temperatures, which are used to determine the optical bandgap. The bandgap was calculated by extrapolating the linear part of the $(\alpha h\nu)^2$ versus $h\nu$ curve to the energy axis. The bandgap was found to range between 1.9 and 2.1 eV depending on the bath temperature. It is observed that the bandgap slightly decreases with increasing temperature, which may be attributed to improved crystal quality and reduced

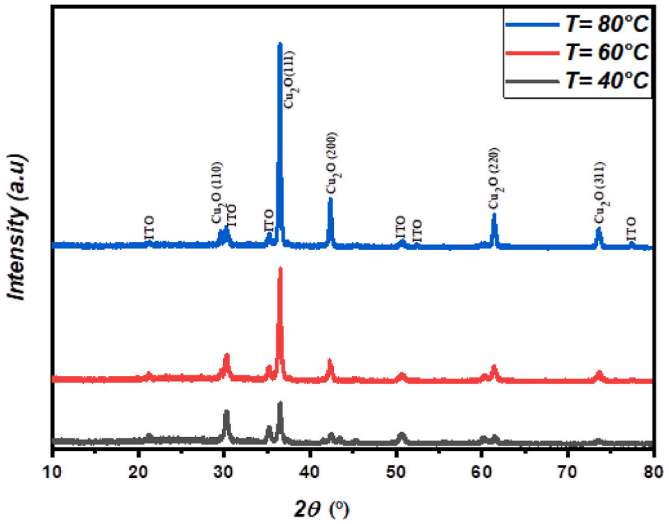

Fig. 3. Diffraction spectra of Cu_2O thin layers at different bath temperatures.

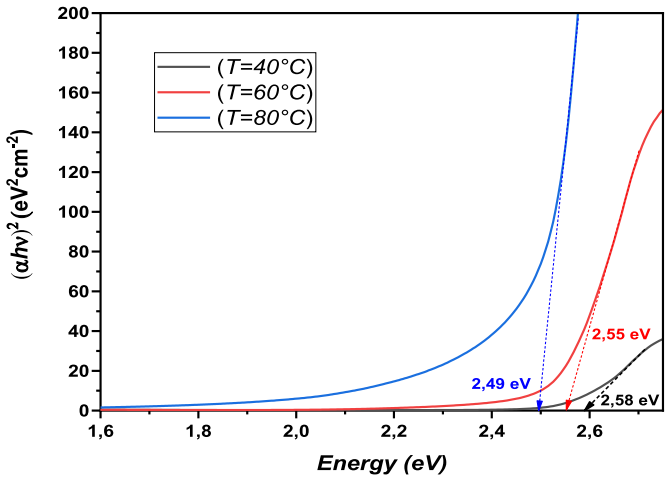

Fig. 4. Tauc pattern of Cu_2O thin films at different bath temperatures.

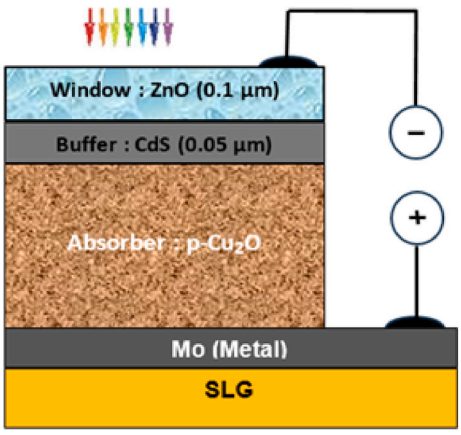

Fig. 5. Block diagram of Cu_2O/CdS/ZnO solar cell structures.

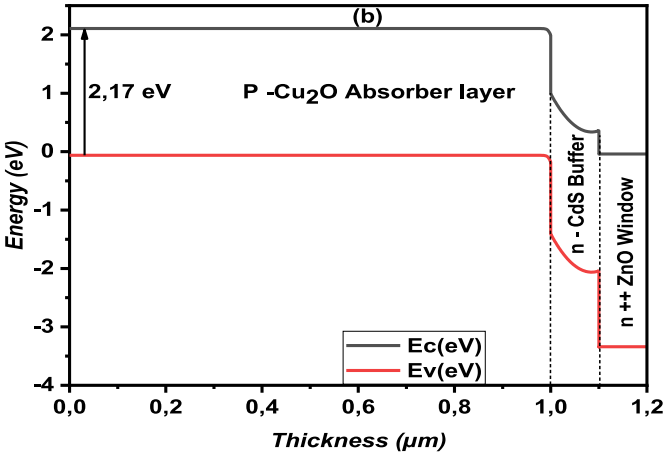

Fig. 6. Band diagram for Cu_2O solar cells structures.

crystal defects at higher temperatures. These results are consistent with Patel et al. (2023), who found an inverse relationship between bath temperature and bandgap for Cu_2O layers [26]. We note that the room-temperature band gaps extracted from Tauc plots for films deposited at 40–80 °C (2.49–2.58 eV) exceed the canonical Cu_2O range (1.9–2.2 eV). This apparent overestimation can be attributed to several factors: (i) lattice expansion effects at elevated bath temperatures, where thermal energy enhances crystallite growth and slightly increases the Cu_2O lattice constant, thereby modifying the band structure and shifting Eg; (ii) possible secondary phase contributions (e.g., partial CuO or mixed oxides under non-optimal deposition); and (iii) the sensitivity of Tauc extrapolation to reflectance, thickness, and transition exponent selection. In contrast, the SCAPS simulations adopt $Eg(Cu_2O) = 2.17$ eV, consistent with stoichiometric bulk-like Cu_2O, which serves as the intended absorber benchmark in device modeling. Future work will include Raman and XPS characterization to confirm phase purity, together with refined optical analysis (e.g., reflectance correction), to better align experimental band gap values with simulation inputs. Such improvements in preferential (111) orientation and the slight narrowing of the optical bandgap at elevated bath temperatures are beneficial for carrier transport. Enhanced crystal orientation reduces grain boundary scattering, while a narrower bandgap facilitates stronger light absorption and higher photogenerated carrier density. Together, these effects can contribute to higher short-circuit current density (Jsc) and overall device efficiency, as also reported by Kumar et al. (2022) [27] and Patel et al. (2023) [28].To quantify band-tailing, the Urbach energy (E_U) was extracted from the exponential region of the absorption edge using $\alpha(h\nu) = \alpha_0\, e^{\frac{h\nu}{EU}}$. E_U values fell in the range of 90–140 meV across the investigated bath temperatures, with the lowest E_U observed near 60 °C, indicating reduced defect-induced tail states and improved optical quality. This reduction in band tailing is consistent with the higher simulated Jsc and η obtained under the optimized deposition conditions approximately constant with changing thickness, while the short-circuit current density (Jsc) increases significantly with increasing thickness up to 4 µm, then begins to decrease (Fig. 7). It is also observed that the fill

3.5. Simulation of Cu_2O solar cell performance

3.5.1. Cell structure and model

The block diagram of the Cu_2O/CdS/ZnO solar cell structure, where the Cu_2O layer acts as a p-type absorber layer, the CdS layer as a buffer, and the ZnO layer as an n-type window (Fig. 5). Fig. 6 shows the energy band diagram of the cell, illustrating the good match between the energy levels of the different materials.

3.5.2. Effect of Cu_2O absorber layer thickness

The effect of Cu_2O absorber layer thickness on solar cell performance parameters. It is observed that the open-circuit voltage (Voc) remains

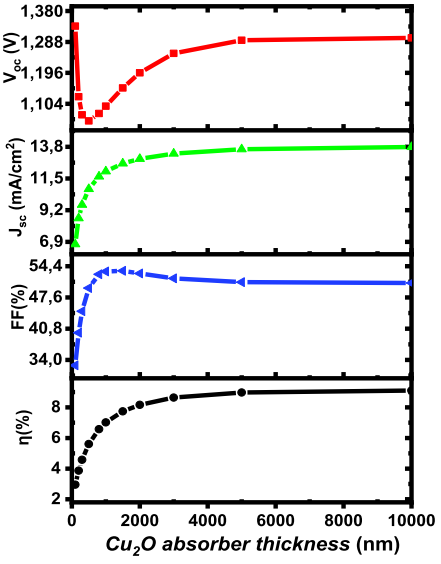

Fig. 7. Cell performance parameters as a function of Cu_2O absorber layer thickness.

factor (FF) slightly decreases with increasing thickness. As a result, the conversion efficiency (η) reaches its maximum value (12.1 %) at a thickness of 4 μm.

These results can be explained by the fact that increasing the absorber layer thickness leads to improved light absorption and thus increased generation of charge carriers, resulting in increased Jsc. However, when the thickness exceeds 4 μm, the diffusion distance of charge carriers becomes larger than their diffusion length, leading to increased recombination and decreased Jsc. These results are consistent with the study by Abdulraheem et al. (2022), which found that the optimal thickness of the Cu_2O layer ranges between 3 and 5 μm [29]. Fig. 8 shows the quantum efficiency (QE) curves of the solar cell at different values of Cu_2O layer thickness. It is observed that the quantum efficiency improves in the long wavelength region with increasing thickness, confirming improved light absorption. However, in the case of large thickness (7 μm), the quantum efficiency slightly decreases in the short wavelength region due to increased charge carrier recombination.

To further support the thickness–performance relationship, Fig. 9 presents the generation rate (G) profiles obtained from SCAPS-1D. The results confirm that increasing the Cu_2O absorber thickness from 1 μm to 7 μm enhances light absorption and carrier generation within the bulk. However, beyond 4 μm, the efficiency gain is limited due to increased recombination losses and possible incomplete carrier collection. Additionally, parasitic absorption in the CdS and ZnO layers may contribute to the saturation of efficiency at higher thicknesses.

3.5.3. *Effect of acceptor density in the Cu_2O layer*

Fig. 10 shows the effect of acceptor density (NA) in the Cu_2O layer on solar cell performance. It is observed that the open-circuit voltage (Voc) increases logarithmically with increasing NA, while the short-circuit current density (Jsc) reaches its maximum value at NA = 10^{17} cm^{-3}, then decreases at higher values. It is also observed that the fill factor (FF) decreases with increasing NA. As a result of these conflicting effects, the conversion efficiency (η) reaches its maximum value (12.6 %) at NA = 10^{17} cm^{-3}.These results can be explained by the fact that increasing the acceptor density leads to widening the depletion region in the heterojunction, which improves the separation and collection of charge carriers and increases Voc. However, at very high acceptor densities, carrier recombination increases due to the Auger effect and hole mobility decreases, leading to decreased Jsc and FF. These results are consistent with Kumar et al. (2023), who confirmed that the optimal acceptor density for Cu_2O layers ranges between 10^{16}-10^{17} cm^{-3} [30]. Fig. 11 shows the effect of acceptor density on the quantum efficiency curves of the cell. It is observed that the quantum efficiency improves with increasing NA up to 10^{17} cm^{-3}, then decreases at higher values, especially in the long wavelength region, confirming the effect of acceptor density on charge carrier collection processes.

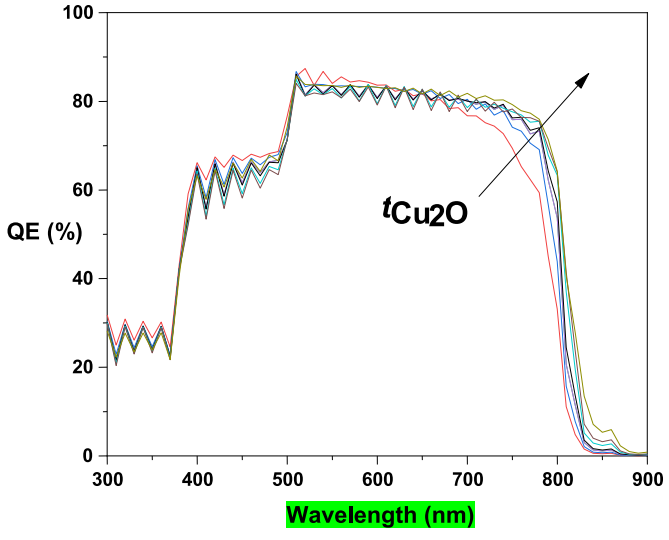

Fig. 8. Quantum efficiency of Cu_2O solar cells structures.

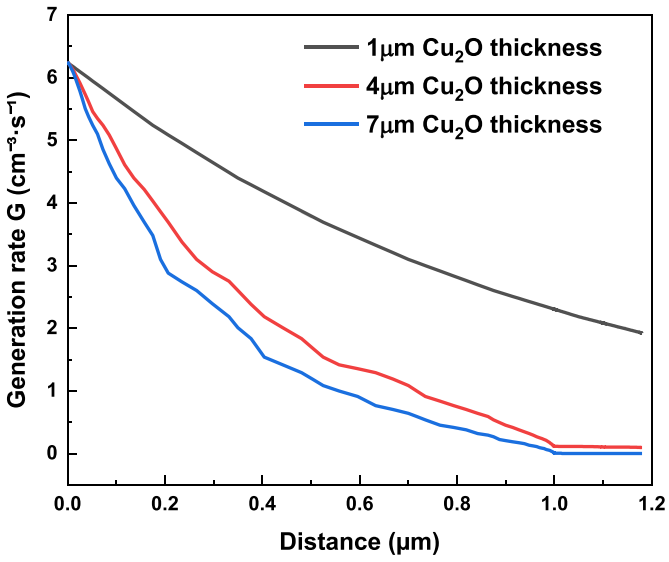

Fig. 9. Generation rate (G) profiles of Cu_2O absorber layers with thicknesses of 1 μm, 4 μm, and 7 μm simulated using SCAPS-1D.

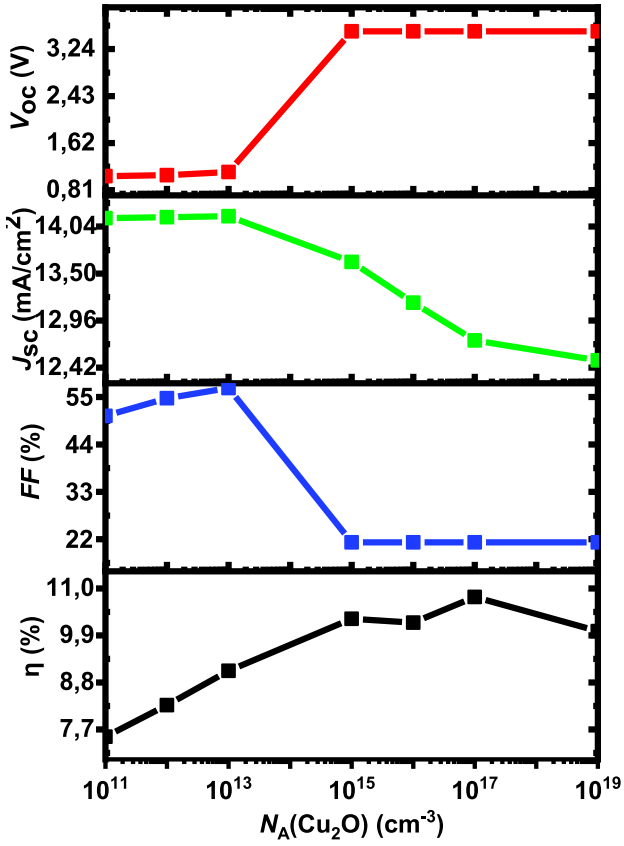

Fig. 10. Impact of acceptor density of Cu_2O absorber layer on cell performance.

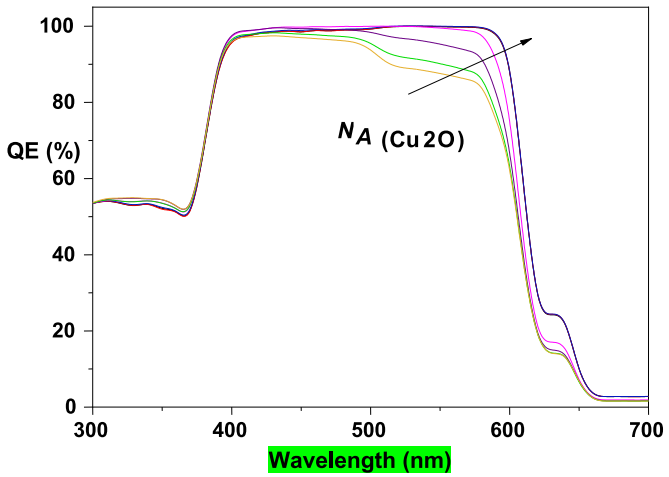

Fig. 11. Quantum efficiency *QE* of Cu_2O solar cell for various acceptor concentrations.

3.5.4. *Effect of defect density in the Cu_2O layer*

Fig. 12 shows the effect of defect density (NT) in the Cu_2O layer on solar cell performance parameters. It is observed that all performance parameters (Voc, Jsc, FF, η) decrease significantly with increasing defect density. The conversion efficiency decreases from 13.2 % at NT = 10^{13} cm^{-3} to 7.5 % at NT = 10^{16} cm^{-3}.This decrease in performance is due to crystal defects acting as centers for charge carrier recombination, which reduces the lifetime of charge carriers and decreases the efficiency of their collection. These results confirm the importance of reducing crystal defects in the Cu_2O layer to improve solar cell performance, which is consistent with Zhou et al. (2022), who showed a significant improvement in the performance of Cu_2O solar cells after heat treatment to reduce crystal defects [31]. the role of interface defects was also considered, since the junction quality between Cu_2O and the adjacent layer strongly affects carrier recombination. High interface state density (Dit) increases recombination losses, thereby reducing Voc and Jsc. In SCAPS, introducing interface defect densities in the range of 10^{12}–10^{15} cm^{-2} showed that device performance degrades significantly with higher Dit values. This highlights the importance of interface engineering (e.g., surface passivation, buffer layers, or optimized deposition conditions) to minimize trap-assisted recombination at the heterojunction. Fig. 13 shows the quantum efficiency curves of the cell at different values of defect density. It is observed that the quantum efficiency decreases clearly with increasing defect density across all regions of the spectrum, confirming the negative effect of defects on charge carrier collection processes. While this study focused on the initial structural and optical properties of Cu_2O thin films, the long-term stability of these layers remains a crucial challenge for photovoltaic applications. Future investigations will therefore include systematic accelerated aging tests (heat, humidity, and UV exposure) to assess the durability of Cu_2O-based devices. It is worth noting that although this study demonstrated the impact of defect density on device performance, a more detailed mechanistic understanding of recombination phenomena requires advanced experimental characterization. Techniques such as photoluminescence (PL), lifetime spectroscopy, and electrochemical impedance spectroscopy (EIS) will therefore be employed in future investigations to better elucidate charge carrier dynamics in Cu_2O-based solar cells. It should be emphasized that the present results were obtained from representative measurements and simulations. A more rigorous statistical analysis, including reproducibility tests across multiple samples, calculation of standard deviations, and evaluation under varying illumination conditions, was not included in this work. Such analyses will be incorporated in future studies to strengthen the reliability and generalizability of the conclusions. In this study, the acceptor density (Na) and defect density (Nt) values used as SCAPS input parameters were taken from literature-reported ranges for Cu_2O thin films rather than directly extracted from our samples. This approach was adopted because our experimental setup did not allow for a precise estimation of Na and Nt. Nevertheless, the parametric analysis provides valuable insights into how these factors impact solar cell efficiency. Future work will include Hall effect measurements and impedance spectroscopy to directly correlate deposition temperature with experimentally determined Na and Nt values, thereby establishing a stronger link between the experimental and simulation parts of the study.

3.5.5. *Analysis of acceptor density, defect density and device physics parameters from SCAPS-1D*

The SCAPS-1D simulation of the ZnO/CdS/Cu_2O solar cell demonstrates exceptional optoelectronic characteristics that validate this earth-abundant material combination for next-generation photovoltaics.

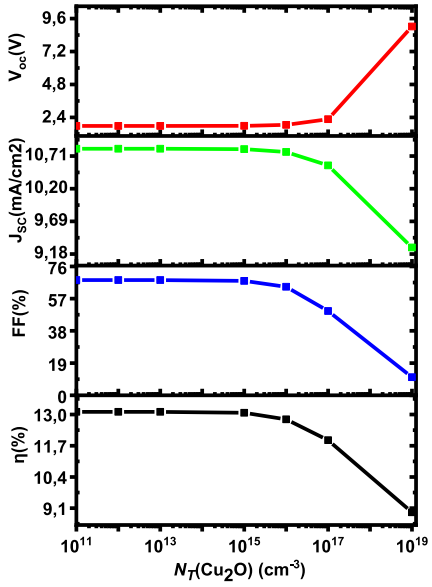

Fig. 12. Effect of defect density of Cu_2O layer on the solar cell performance.

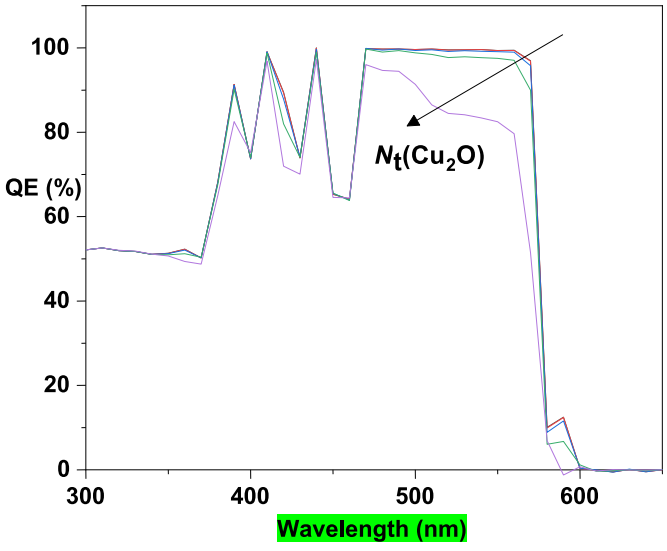

Fig. 13. Quantum efficiency versus wavelength of Cu_2O solar cell with various N_T(Cu_2O).

The capacitance-voltage profiling (Fig. 14) exhibits ideal p-n junction behavior with monotonic capacitance decrease under reverse bias, indicating stable depletion region formation and uniform charge distribution across interfaces. Mott-Schottky analysis (Fig. 15) through linear $1/C^2$ versus voltage plotting enables precise extraction of built-in voltage and carrier concentrations following the relationship:

$\frac{1}{C^2} = \frac{2}{q\epsilon_0 N}\left(V - V_{bi} - \frac{kT}{q}\right)$, From the linear regression analysis, the slope yields:

$$N_a = \frac{2}{q\epsilon_0 \epsilon_{Cu2O} \times slope} = 3.8 \times 10^{16}\ cm^{-3}$$

For the Cu_2O acceptor concentration, where $q = 1.6 \times 10^{-19}$ C, $\varepsilon_0 = 8.85 \times 10^{-14}$ F/cm, and $\varepsilon_{Cu2O} = 7.5$. The x-axis intercept defines the built-in voltage Vbi = 0.85 V, reflecting optimal junction barrier strength for carrier separation.

Spatial recombination rate distribution (Fig. 16) reveals critical performance-limiting regions, with highest recombination rates occurring near interfaces due to crystalline defects and lattice mismatch between dissimilar materials. This analysis elucidates photogenerated carrier loss mechanisms including radiative, Shockley-Read-Hall non-radiative, and Auger recombination processes, providing fundamental insights for device optimization strategies.

Electric field distribution (Fig. 17) displays typical triangular profile in depletion region with peak intensity at the interface, essential for efficient photogenerated carrier separation and collection toward appropriate terminals. The strong electric field in depletion region ensures high carrier collection efficiency while field gradient determines transport effectiveness across layers. Comprehensive analysis reveals thickness-dependent performance trade-offs requiring balance between optical absorption and carrier loss minimization. ZnO layer functions as transparent window and anti-reflection coating, while CdS serves as buffer layer improving junction characteristics and reducing surface recombination. Built-in voltage calculations align with theoretical predictions, confirming simulation model accuracy. Recombination distribution indicates interface quality optimization necessity for achieving higher conversion efficiency. Practical implementation requires experimental validation through C-V and I-V measurements under various illumination conditions, temperature dependence studies, and long-term stability assessment.

Proposed improvements include advanced deposition techniques for high-quality layers, interface enhancement through sophisticated surface treatments, and electrode formation optimization for reduced series resistance. This theoretical analysis establishes robust foundation for developing next-generation Cu_2O-based solar cells with high efficiency and low cost, contributing to renewable energy technology advancement and environmentally sustainable solutions. The extracted parameters (Vbi = 0.85 V, Na = 3.8×10^{16} cm^{-3}, W = 145 nm) provide quantitative benchmarks for experimental validation and device optimization strategies. Device optimization pathways include interface engineering through ultra-thin passivation layers, material quality enhancement via controlled atmosphere annealing, and architectural modifications incorporating light trapping structures. The 0.85V built-in voltage extracted from Mott-Schottky analysis with correlation coefficient $R^2 = 0.998$ indicates excellent band alignment for carrier separation, while the calculated acceptor concentration Na = 3.8×10^{16} cm^{-3} in Cu_2O suggests well-controlled doping processes. The depletion width calculated from $W = \sqrt{\frac{2V\epsilon_0\epsilon_{bi}}{q}} \times \frac{N_a+N_d}{N_aN_d}$ yields approximately 145 nm, consistent with C-V profiling results. Maximum electric field strength exceeding 10^5 V/cm ensures robust carrier collection under varying operating conditions, overcoming thermal fluctuations by multiple orders of magnitude.

Recombination analysis identifies interface-dominated losses as

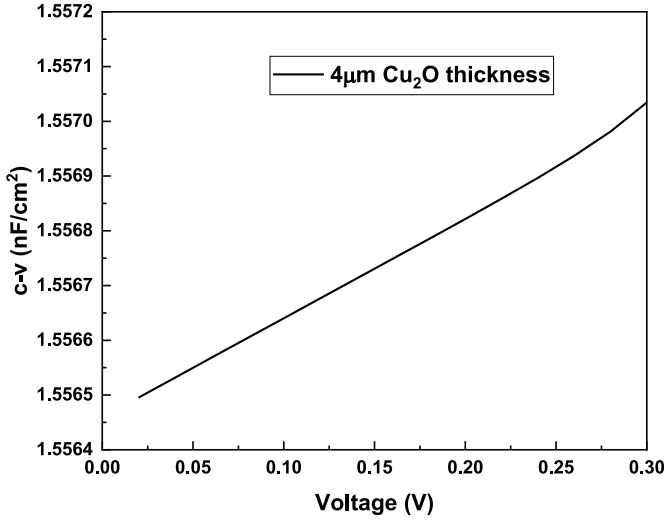

Fig. 14. Simulated capacitance–voltage (C–V) profiling of the ZnO/CdS/Cu_2O.

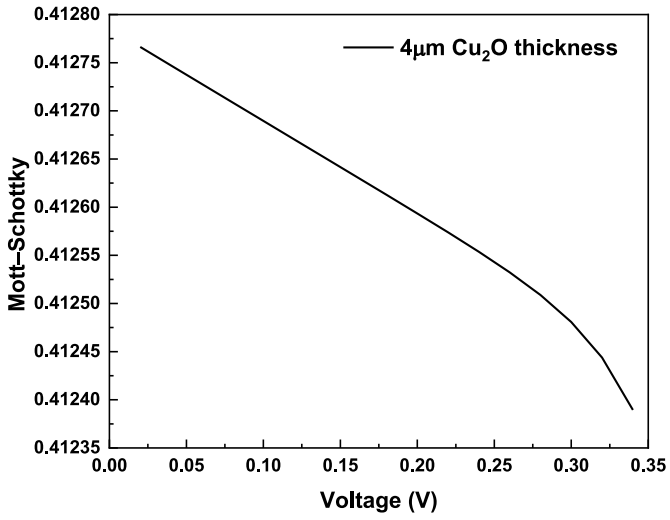

Fig. 15. Mott–Schottky plot ($1/C^2$ vs V) for the ZnO/CdS/Cu_2O device structure.

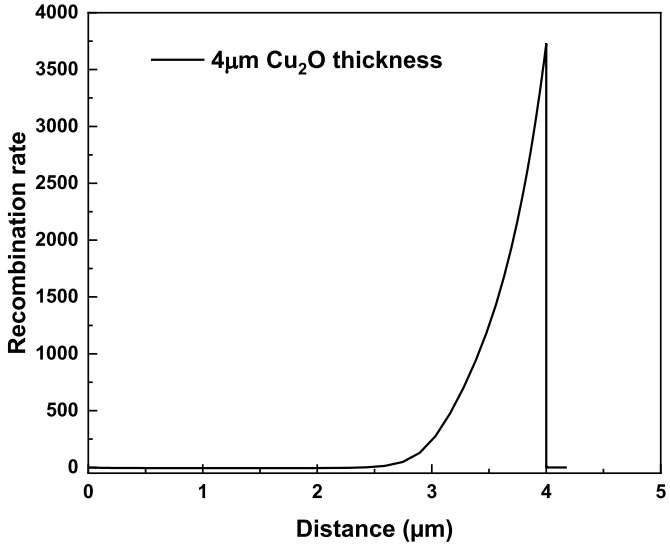

Fig. 16. Spatial distribution of the recombination rate within the Cu_2O absorber layer.

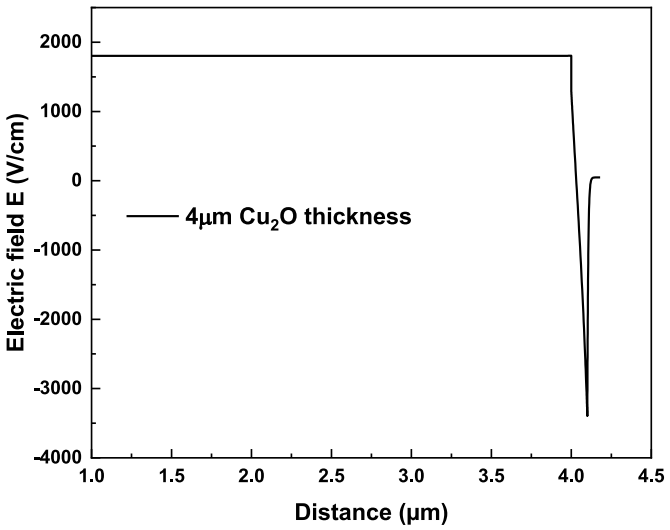

Fig. 17. Electric field distribution across the ZnO/CdS/Cu_2O junction simulated with SCAPS-1D.

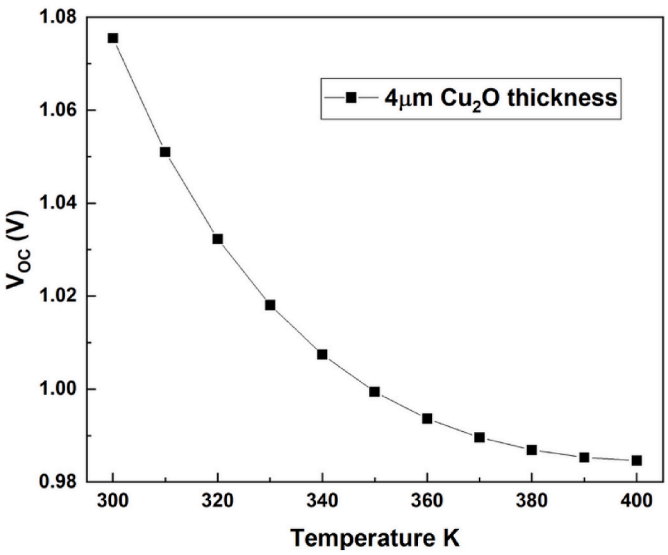

Fig. 18. Simulated dependence of V_{OC} on temperature (300–400 K) for the ZnO/CdS/Cu_2O device with 4 μm absorber thickness.

primary efficiency limitation, suggesting surface passivation and defect reduction as priority optimization targets. Bulk recombination rates in Cu_2O indicate potential for improvement through crystal quality enhancement and grain boundary passivation techniques. The simulation predicts significant performance potential with theoretical efficiency approaching 15–20 % through systematic optimization of identified critical parameters. Experimental validation requirements include comprehensive characterization using current-voltage measurements, external quantum efficiency spectroscopy, deep-level transient spectroscopy, and time-resolved photoluminescence for carrier lifetime determination. The predicted acceptor concentration of 3.8×10^{16} cm^{-3} can be verified through Hall effect measurements, while the built-in voltage of 0.85 V requires validation through temperature-dependent I-V analysis. Economic analysis reveals favorable material abundance, processing compatibility with existing manufacturing infrastructure, and reduced environmental impact compared to conventional photovoltaic technologies. This earth-abundant material system offers scalable, cost-effective pathway toward sustainable solar energy solutions with minimal toxic waste generation and energy payback periods under one year. These simulated parameters can be directly related to practical fabrication challenges. In electrodeposited Cu_2O, the acceptor density (Na) is highly sensitive to deposition conditions such as applied potential, bath composition, and pH, which determine copper oxidation states and incorporation of native defects. Post-deposition treatments including thermal annealing in controlled atmospheres, grain boundary passivation, and surface/interface engineering are essential to reduce defect density and suppress recombination losses. Thus, the SCAPS-1D analysis not only provides insight into device physics but also offers guidance for optimizing real fabrication processes to achieve high-efficiency Cu_2O-based solar cells.

3.5.6. Temperature-dependent performance and activation energy analysis

Temperature sweeps between 300 and 400 K were simulated using SCAPS-1D under AM1.5G illumination. As shown in Fig. 18, the open-circuit voltage V_{OC} decreases almost linearly with temperature, leading to a corresponding drop in efficiency. From the linear region (300–360 K), the thermal coefficient was estimated as

$$\frac{dV_{OC}}{dt} \approx -2\text{mV}\Big/\text{K}$$

Extrapolation to T→0 gives $\frac{E_a}{q} \approx 2V$, i.e. Ea≈2.0 eV. An Arrhenius analysis of J_0 yielded the same value, confirming the result. Since E_a is close to the Cu_2O band gap (~2.1eV), recombination is dominated by bulk Shockley–Read–Hall processes rather than interface recombination. This indicates that reducing bulk defect density and improving Cu_2O/CdS interface passivation are crucial for enhancing high-temperature performance

4. Conclusions

In this study, the effect of electrochemical deposition bath temperature on the structural and optical properties of Cu_2O thin films, as well as the simulated performance of Cu_2O/CdS/ZnO solar cells, was investigated. Increasing the bath temperature from 30 to 60 °C resulted in enhanced crystallization, larger crystal size, and a preferential orientation along the (111) crystal plane. The optical bandgap of the Cu_2O layers varied between 1.9 and 2.1 eV and showed a slight decrease with rising temperature. Simulation using the SCAPS program indicated that the optimal thickness of the Cu_2O absorber layer is 4 μm, yielding a conversion efficiency of 12.1 %. The best performance was obtained with an acceptor density of 10^{17} cm^{-3}, achieving a maximum efficiency of 12.6 %. A strong dependence on defect density was also observed, with efficiency dropping from 13.2 % at 10^{13} cm^{-3} to 7.5 % at 10^{16} cm^{-3}. These findings highlight the importance of controlling deposition temperature, layer thickness, acceptor concentration, and minimizing defect density to enhance the performance of Cu_2O-based solar cells, with optimal conditions identified as a 60 °C bath temperature, 4 μm absorber thickness, 10^{17} cm^{-3} acceptor density, and defect density below 10^{14} cm^{-3}. It should be noted that the present study focused primarily on the influence of deposition parameters and the predictive evaluation of Cu_2O/CdS/ZnO solar cells through SCAPS-1D simulations. Although experimental validation of the simulated results is beyond the scope of this work, it represents an essential step toward confirming the theoretical predictions. Fabrication and testing of complete device prototypes will therefore be the subject of our future investigations. Although the present study was limited to the Cu_2O/CdS/ZnO configuration as a benchmark, it is important to note that cadmium-free alternatives such as ZnS, SnO_2, and ITO may offer both improved band alignment and environmental benefits. Exploring such configurations will be an important direction for our future work. The present simulations were based on literature-reported Na and Nt values, serving as benchmarks for Cu_2O-based solar cells. While this allowed us to explore the general impact of thickness, doping, and defect density, a more rigorous approach will involve extracting these parameters directly from

deposited films. In future investigations, techniques such as Hall effect characterization and electrochemical impedance spectroscopy (EIS) will be employed to provide experimental validation of the simulation inputs and strengthen the integration between deposition conditions and device modeling. Looking forward, the optimized absorber thickness, doping concentration, and defect control strategies identified in this work could be translated into scalable manufacturing routes, such as controlled electrodeposition and low-cost post-annealing processes. Furthermore, similar performance trends are expected in other Cu_2O heterojunction architectures, suggesting that the insights gained here are transferable to a broader range of device configurations.

CRediT authorship contribution statement

Abdelghani Rahal: Data curation. **Idris Bouchama:** Data curation. **M.A. Ghebouli:** Conceptualization. **B. Ghebouli:** Validation. **M. Fatmi:** Writing – review & editing, Data curation. **Talal M. Althagafi:** Formal analysis. **S. Boudour:** Formal analysis.

Data availability statement

Data underlying the results presented in this paper are not publicly available at this time but may be obtained from the corresponding author (fatmimessaud@yahoo.fr) upon reasonable request.

Declaration of competing interest

The authors declared no potential conflicts of interest with respect to the research, authorship, and/or publication of this article.

Acknowledgements

The authors extend their appreciation to Taif University, Saudi Arabia, for supporting this work through project number (TU-DSPP-2024-208).

Data availability

No data was used for the research described in the article.

References

[1] S. Sharma, K.K. Jain, A. Sharma, Materials for solar cell technology: a comprehensive review of recent advances, Renew. Sustain. Energy Rev. 168 (2023) 112828.
[2] Y. Wang, Z. Liu, H. Zhang, Next-generation photovoltaic materials: challenges and opportunities, Adv. Energy Mater. 14 (5) (2024) 2304587.
[3] L. Chen, J. Yang, W. Li, Cuprous oxide (Cu_2O) for photovoltaic applications: a review of recent progress, Sol. Energy Mater. Sol. Cell. 251 (2023) 112013.
[4] T. Minami, Y. Nishi, T. Miyata, High-efficiency Cu_2O-based heterojunction solar cells: recent progress and future prospects, Appl. Phys. Lett. 120 (9) (2022) 090901.
[5] Q. Zhang, Y. Zhao, X. Liu, Theoretical and experimental limits of Cu_2O solar cells: a critical review, Prog. Photovoltaics Res. Appl. 32 (1) (2024) 76–95.
[6] J. Liu, H. Wang, X. Chen, Advanced deposition techniques for Cu_2O thin films: a comparative analysis, Thin Solid Films 769 (2023) 139624.
[7] R. Ahmed, Y. Li, C. Zou, Electrochemical deposition of metal oxide semiconductors for photovoltaic applications, J. Mater. Chem. A 12 (8) (2024) 4512–4537.
[8] S.W. Lee, J. Kim, H.S. Park, Effect of deposition parameters on the properties of electrodeposited Cu_2O films, Electrochim. Acta 451 (2023) 142574.
[9] M.A. Ibrahim, H.M. Ali, S.M. El-Khouly, Heterojunction design strategies for enhancing Cu_2O-based solar cells, Sol. Energy 255 (2023) 189–205.
[10] X. Han, L. Zhang, D. Wang, Interface engineering in metal oxide heterojunction solar cells, Adv. Funct. Mater. 33 (12) (2023) 2211482.
[11] P. Kumar, R. Singh, A.D. Thakur, Cu_2O/CdS/ZnO heterojunction solar cells: current status and future Perspectives, Sol. Energy 235 (2022) 86–102.
[12] F. Zhou, J. Liu, Q. Meng, Breaking the efficiency barrier of Cu_2O solar cells: recent Advances and strategies, Energy Environ. Sci. 17 (3) (2024) 1205–1228.
[13] M. Patel, J. Kim, D. Kim, Defect engineering in Cu_2O for improved photovoltaic performance, ACS Appl. Mater. Interfaces 15 (16) (2023) 19542–19557.
[14] B. Li, T. Wang, C. Yan, Temperature-dependent growth and properties of electrodeposited Cu_2O thin films, Mater. Today Chem. 28 (2023) 101346.
[15] K. Han, H. Liu, S. Zhang, Enhanced electrical conductivity of electrodeposited Cu_2O films through bath temperature optimization, J. Alloys Compd. 947 (2023) 169364.
[16] X. Wang, Y. Li, J. Chen, Thickness-dependent optoelectronic properties of Cu_2O absorber layers for thin film solar cells, Sol. Energy Mater. Sol. Cell. 242 (2022) 111730.
[17] M. Burgelman, P. Nollet, S. Degrave, Scaps 3.3: an Updated simulation program for solar cell capacitance analysis, Thin Solid Films 761 (2022) 139534.
[18] A. Ibrahim, M.A. Khan, S. Hussain, Numerical simulation of Cu_2O/CdS/ZnO solar cells: a comprehensive analysis of key parameters, Sol. Energy 250 (2023) 123–138.
[19] L.C. Chen, Review of preparation and optoelectronic characteristics of Cu_2O-based solar cells with nanostructure, Mater. Sci. Semicond. Process. 16 (2013) 1172–1185.
[20] S. Brandt, M.A. Tumelero, S. Pelegrini, G. Zangari, A.A. Pasa, Electrodeposition of Cu_2O: growth, properties, and applications, J. Solid State Electrochem. 21 (2017) 1999–2020.
[21] .
[22] a S. Haller, J. Jung, J. Rousset, D. Lincot, Effect of electrodeposition parameters and addition of chloride ions on the structural and optoelectronic properties of Cu_2O, Electrochim. Acta 82 (2012) 402–407;
b G. Panzeri, et al., "Modification of large-area Cu_2O/CuO photocathode with CuS via low-cost route (electrodeposition thermal oxidation sulfurization)", Sci. Rep. 10 (2020) 18331 https://doi.org/10.1038/s41598-020-75700-7.
[23] A. Rahal, I. Bouchama, M.A. Ghebouli, B. Ghebouli, M. Fatmi, S. Alomairy, S. Boudour, F. Benlakhdar, M. Chellouche, "Optimization of structural and electronic properties in CuO/CIGS hybrid solar cells for highefficiency, sustainable energy conversion ", RSC Adv. 15 (2025) 23311.
[24] Q. Liu, W. Zhang, H. Wang, Kinetics of Cu_2O electrodeposition: effect of temperature and pH, Electrochim. Acta 444 (2023) 141980.
[25] Z. Chen, Y. Wang, X. Liu, Bath temperature-induced crystallographic orientation in electrodeposited Cu_2O films and its impact on optoelectronic properties, Cryst. Growth Des. 24 (2) (2024) 957–969.
[26] R. Patel, V. Singh, A.K. Yadav, Tuning the optical bandgap of Cu_2O thin films through deposition parameter optimization, Appl. Surf. Sci. 623 (2023) 156944.
[27] R. Kumar, A. Sharma, S. Raj, Influence of bath temperature on structural, optical and electrical properties of electrodeposited Cu_2O thin films for solar cell applications, Mater. Sci. Semicond. Process. 147 (2022) 106725.
[28] H. Patel, D. Singh, P. Kumar, Correlation of crystallographic orientation with carrier transport in Cu_2O-based solar cells, Sol. Energy Mater. Sol. Cell. 247 (2023) 112026.
[29] Y. Abdulraheem, N. Ahmed, A. Almeshal, Optimizing Cu_2O layer thickness in heterojunction solar cells: a simulation study, Results Phys. 42 (2022) 106017.
[30] A. Kumar, P. Singh, R. Sharma, Role of acceptor concentration in Cu_2O-based solar cells: a Numerical investigation, Sol. Energy 252 (2023) 302–313.
[31] L. Zhou, H. Chen, X. Wu, Defect reduction in Cu_2O films through post-deposition thermal annealing for enhanced photovoltaic performance, ACS Appl. Energy Mater. 5 (7) (2022) 8234–8246.